Low-Cost Battery Monitoring by Converter-Based Electrochemical Impedance Spectroscopy

R. Ferrero, C. Wu
Dept. of Electrical Engineering and Electronics
University of Liverpool, Liverpool, UK
Email: Roberto.Ferrero@liverpool.ac.uk
C.Wu15@liverpool.ac.uk

M. De Angelis, H. George-Williams, E. Patelli
Institute for Risk and Uncertainty
University of Liverpool, Liverpool, UK
Email: Marco.De-Angelis@liverpool.ac.uk
H.George-Williams@liverpool.ac.uk
Edoardo.Patelli@liverpool.ac.uk

A. Carboni, S. Toscani
Dip. di Elettronica, Informazione e Bioingegneria
Politecnico di Milano, Milano, Italy
Email: alberto.carboni@polimi.it
sergio.toscani@polimi.it

P. A. Pegoraro
Department of Electrical and Electronic Engineering
University of Cagliari, Cagliari, Italy
Email: paolo.pegoraro@diee.unica.it

***Abstract*—The use of batteries and other electrochemical devices in modern power systems is rapidly increasing, with stricter requirements in terms of cost, efficiency and reliability. Innovative monitoring solutions are therefore urged to allow a successful development of a wide range of emerging applications, including electric vehicles and large-scale energy storage to support renewable energy generation. Presently, a huge gap still exists between the accurate and sophisticated monitoring techniques commonly employed in laboratory tests, on the one hand, and the simple and rough solutions available in most commercial applications, on the other hand. The objective of this paper is therefore to contribute to the development of low-cost but accurate solutions for commercial battery condition monitoring, by proposing an embedded system that combines real-time digital signal processing with the high computational power and user friendly interface of a modern computer, at a cost comparable to a simple micro-controller. In more detail, the paper focuses on electrochemical impedance spectroscopy on a battery performed by a DC-DC power converter, and it explains how the proposed low-cost off-the-shelf hardware can control the converter, acquire the measurement signals, accurately process them in the time and frequency domains, and estimate the result uncertainty in real-time, which is necessary to promptly and reliably detect any variation in the battery condition.**

***Index Terms*—Batteries, Battery management systems, Electrochemical devices, Electrochemical impedance spectroscopy, Condition monitoring, State estimation, DC-DC power converters**

I. Introduction

Batteries and more generally electrochemical power sources are playing an increasingly important role in modern power systems, driven by the wider use of renewable energy and allowed by the recent developments in electrochemical technology [1]. Battery use is no longer limited to low-power devices, as many emerging applications nowadays include large-scale energy storage for renewable energy generation and powertrain for electric or hybrid vehicles, just to mention a few examples.

Despite the impressive advancements in battery technology in recent years, further improvements are still much needed in key aspects for commercial applications, namely efficiency, reliability and cost. While most of the efforts toward such improvements are focused on battery design and material technology, in-situ monitoring systems also play a very important role. In fact, a more accurate state estimation of the battery internal conditions would allow, on the one hand, a better power management (therefore higher overall efficiency of the power system) and, on the other hand, a more accurate and prompter diagnosis of performance degradation processes (therefore a more reliable operation). If all this were achieved at negligible additional instrumentation cost, the decrease in the overall operation and maintenance costs would lead also to large economic benefits.

Electrochemical impedance spectroscopy (EIS) is a very powerful non-invasive measurement technique, commonly employed in laboratory experiments, which provides a wealth of diagnostic information about electrochemical processes occurring within batteries (and fuel cells as well). The main advantage compared to DC voltage and current measurements alone is that EIS allows distinguishing between different processes and different causes of voltage drop, as they affect the impedance spectrum in different frequency ranges, from millihertz to kilohertz [2]. Several works in the literature have demonstrated how EIS can be effectively employed to accurately estimate the battery state of charge (SOC) and state of health (SOH) [2]–[6]. Nevertheless, the use of EIS in commercial applications is still hindered by the high instrumentation cost and the poor accuracy of results obtained by low-cost solutions. Indeed, commercial applications cannot afford the expensive and sophisticated instrumentation used in the laboratory, such as frequency response analyzers, and as a result, in most cases only DC voltages and currents are monitored, on individual cells or on groups of cells, but in any

case with limited capability of providing accurate and reliable information about the state of the battery, particularly the SOH.

The use of power converters has been recently suggested as a possible solution to achieve EIS in commercial applications at lower cost. Power converters represent a very promising solution because they are already available in most applications and, if properly controlled, they can introduce AC perturbations superimposed to the battery DC current and voltage, at the desired frequencies to measure the impedance spectrum in relevant frequency ranges [7]. This solution would not require any additional hardware to create the AC perturbations, although it may require additional hardware to implement the necessary advanced features for the power converter control and to acquire and process the current and voltage measurements.

A number of papers have appeared in the literature in the last few years, reporting the results of preliminary feasibility studies applied to batteries [8]–[12], as well as to fuel cells [13]–[15]. The solutions presented in the literature so far are, however, still affected by important limitations, mainly arising from the need to find a balance between high accuracy of results, on the one hand, and the use of simple and inexpensive hardware, on the other hand. In the simplest solution [9], the voltage and current signals are processed in the time domain, by measuring their peak-to-peak amplitudes and the time delay between the two waveforms, which leads to much less accurate results compared to a frequency-domain analysis in presence of noise or distortions. Even when the signals are processed in the frequency domain, the AC perturbation is often just a sine wave and allows measuring the impedance at one frequency at a time [8], [10], [11], whereas a multi-sine perturbation would be very useful to dramatically decrease the measurement time and obtain more accurate impedance spectra. Moreover, in most cases the perturbations are added by modulating the converter duty cycle by a sinusoidal oscillation, instead of directly controlling the battery current or voltage, and this may lead to significant distortions in the waveforms. Finally, the visualization and post-processing of impedance spectra requires communication with external hardware and software when a simple FPGA is employed for signal acquisition and power converter control [12].

The objective and new contribution of this paper are therefore the design of a fully embedded solution for converter control, signal acquisition and processing, and state estimation, entirely based on a low-cost off-the-shelf hardware platform that combines hard real-time signal generation and acquisition with the processing capability and the user friendly visualization tools of a modern computer. Such a solution has the potential to allow not only real-time impedance measurements in a wide frequency range, as required for battery condition monitoring, but also real-time evaluation of the measurement uncertainty, which is necessary to promptly and reliably detect any variation in the battery condition and to accurately estimate equivalent parameters by fitting the measured impedance values with appropriate models.

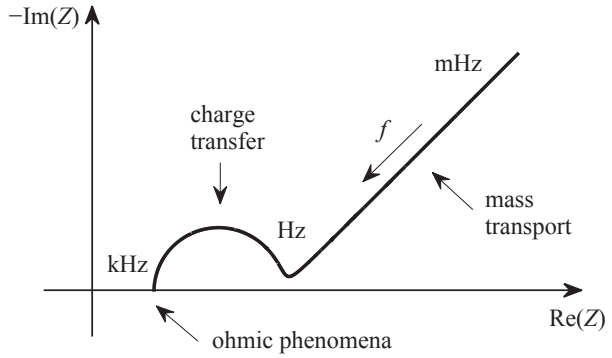

Fig. 1. Typical impedance spectrum of a battery, in a frequency range from millihertz to kilohertz, revealing different electrochemical processes.

II. Battery SOC and SOH Estimation by EIS

The battery state and behavior are characterized by the interplay of a large number of physical processes, occurring on very different time scales, from microseconds to years [2]. EIS measurements can typically cover a frequency range down to millihertz or slightly below, therefore the impedance spectrum includes the effects of three main processes, namely ohmic phenomena (in the kilohertz range), charge transfer in the electrochemical double layer (in the hertz range) and mass transport of ions (in the millihertz range). Fig. 1 shows the Nyquist diagram of a typical spectrum, where the three phenomena above can be clearly distinguished.

The impedance spectrum can be interpreted in terms of an equivalent electrical circuit, where each impedance is associated with a different process and represents a different contribution to the overall voltage drop (and losses, in case of resistive components). Several equivalent circuits can be found in the literature, of different type and complexity, used to model different batteries in different conditions, but a simple and common circuit approximately valid for all battery types is illustrated in Fig. 2, where R_{ohm} represents the ohmic losses, R_{t} and C_{t} represent the charge double layer, and Z_{w} (called Warburg impedance) represents the mass transport and is defined by the following expression:

$$Z_{\mathrm{w}}\left(j\omega\right) = \sigma_{\mathrm{w}} \frac{1-j}{\sqrt{\omega}} \tag{1}$$

Processes occurring on longer time scales, such as those due to a change in the SOC or due to aging (deterioration of SOH) can be detected as changes in the values and shape of the spectrum and can be interpreted in terms of changes in one or more of the equivalent circuit parameters, although the relationship may not always be straightforward. In lithium-ion batteries, the SOC does not significantly affect the ohmic resistance while it mainly affects the mass transport and, to a lower extent, the charge transfer [2]–[4], whereas in lead-acid batteries the SOC affects also the ohmic resistance [6]; in both battery types, however, the main variations are visible

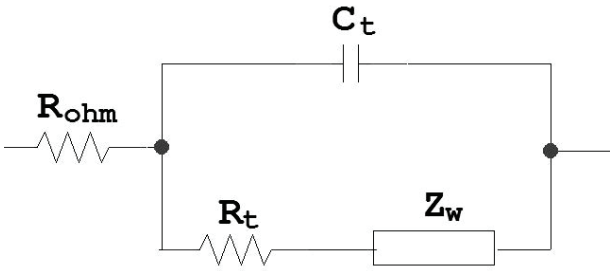

Fig. 2. Equivalent circuit of the battery impedance, corresponding to the impedance spectrum shown in Fig. 1.

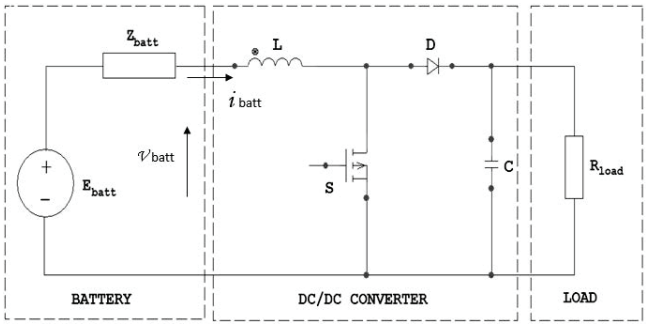

Fig. 3. Equivalent circuit of the designed power system prototype, composed of a battery (with its impedance that has to be measured), a DC-DC boost converter and a resistive load.

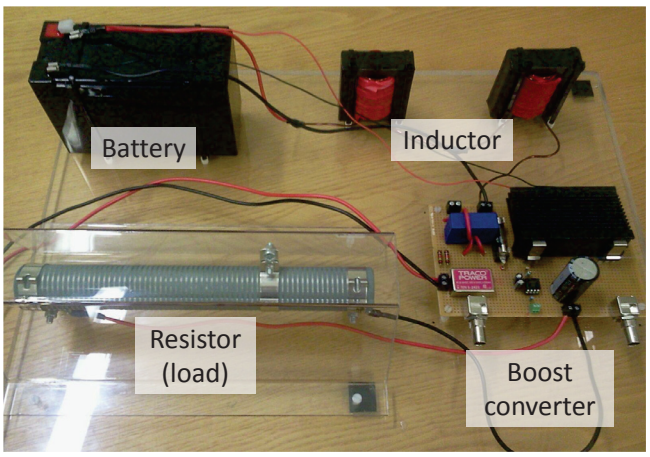

Fig. 4. Photograph of the prototype used for the tests, composed of a lead-acid battery, a home-made DC-DC converter and a resistive load.

in the low-frequency part of the impedance spectrum. On the other hand, the SOH affects the whole spectrum, at high and low frequencies, in both lithium-ion [2], [3] and lead-acid [6] batteries, with different parts of the spectrum being more or less influenced by different causes of performance degradation and aging.

The use of EIS to accurately estimate the battery SOC and SOH requires therefore the measurement of the impedance spectrum in a wide frequency range, down to the millihertz region, thus with a very long measurement time which is extremely challenging, particularly in commercial applications, because the battery is unlikely to remain in steady-state conditions during such a long time. For this reason, a classic Fourier approach may lead to highly inaccurate results, and more sophisticated algorithms combining time-domain and frequency-domain analysis should be used to compensate for changes in the operating conditions or internal state of the battery [16]. A real-time evaluation of the uncertainty of the measured impedance would also be useful to know whether each measured data can be used or should be discarded, e.g. because of too big changes in the battery condition occurred during the measurement itself.

III. Hardware Design and Experimental Setup

A. DC-DC Boost Converter

The proposed methodology is tested on a switch-mode DC-DC boost converter, as batteries are low-voltage, high-current sources and in most applications their voltage has to be boosted to match the load requirements or to decrease the energy transmission losses. A converter prototype was specifically designed and assembled for this purpose, instead of using a commercial product, in order to have a full control over the converter and be able to customize the switch control strategy according to the aim of the paper.

The equivalent circuit of the whole power system, composed of source, converter and load, is illustrated in Fig. 3, while a photograph of the prototype is shown in Fig. 4. The chosen battery is a 12 V, 7 Ah sealed lead-acid battery composed of 6 cells in series, and the boost converter was designed for a primary (battery) rated current of 10 A. A variable resistor with 10 Ω maximum resistance is used as the load for sake of simplicity. Because of the low power of the circuit, the controlled switch is a MOSFET, and the converter was designed to operate with pulse width modulation (PWM) control at switching frequencies between 10 kHz and 100 kHz. The board also includes a LEM LA 25-P closed-loop Hall-effect current transducer, with a frequency bandwidth from 0 to 200 kHz, used to measure the battery current.

When the converter operates in continuous conduction mode, the ideal (without losses) relationship between input and output voltages is:

$$V_{\mathrm{o}} = \frac{V_{\mathrm{i}}}{1-\delta} \tag{2}$$

where V_{i} and V_{o} are the DC (or slowly changing, compared to the switching period) voltages and δ is the converter duty cycle, i.e. the fraction of the switching period when the switch is on. The switching frequency f_{sw} and duty cycle δ affect also the peak-to-peak amplitudes of the input current ripple ΔI_{i} and output voltage ripple ΔV_{o}, and the consequent design of the input inductance L and output capacitance C. Again, in ideal conditions, the following equations are derived, respectively:

$$\Delta I_{\mathrm{i}} = \frac{V_{\mathrm{i}}\delta}{L f_{\mathrm{sw}}} \tag{3}$$

$$\Delta V_{\mathrm{o}} = \frac{I_{\mathrm{i}}\,(1-\delta)\,\delta}{C f_{\mathrm{sw}}} \tag{4}$$

Based on (3) and on the rated input voltage (12 V) and current (10 A), an inductance L = 1.2 mH was chosen to guarantee a peak-to-peak input current ripple below 10% of the DC current at f_{sw} = 10 kHz and below 1% at f_{sw} = 100 kHz. Similarly, based on (4), a capacitance C = 470 μF was chosen to guarantee a peak-to-peak output voltage below 3% of the DC voltage at f_{sw} = 10 kHz and below 0.3% at f_{sw} = 100 kHz.

The switch control, described in the next subsection, allows controlling the duty cycle on time scales of tens of microseconds, in order to introduce AC perturbations at frequencies up to a few kilohertz, depending on the chosen switching frequency. This converter is therefore suitable to measure the full impedance spectrum of the battery, as illustrated in the previous section.

B. Signal Acquisition, Generation and Processing

The hardware required to implement the proposed impedance measurement technique must have hard real-time processing capability to control the converter operation and to acquire the voltage and current measurement signals, and at the same time it must have a large computational power to implement signal processing and state estimation algorithms in the time and frequency domains, with real-time uncertainty evaluation, and a graphical interface to effectively diplay results to the user. Last but not least, such hardware should be also simple to use, inexpensive and compact, in order to be easily applied to commercial applications, and flexible enough to be customized to accommodate different measurement requirements in terms of accuracy, number of channels, etc.

According to these considerations, a BeagleBone Black (BBB) board, shown in Fig. 5, appears to be an appropriate choice. The BBB is a low-cost (around $50) development board that includes a Texas Instruments 1-GHz AM3358 ARM Cortex-A8 processor (supporting several open-source operating systems, such as Linux), as well as 2 separate 200-MHz programmable real-time units (PRUs), sharing the same data bus with the ARM processor, thus allowing a simple and fast exchange of data. The BBB features a number of digital input-output channels, including PWM outputs suitable for the converter switch control. The board also includes an 8-channel, 12-bit, 200-kSa/s analog-to-digital converter (ADC), which is suitable to acquire the battery voltage and current signals with appropriate sampling frequency and resolution. If, however, a particular application requires (and can afford) more accurate measurements or more channels, it is possible to add external ADCs to the board, connected through a serial interface (SPI), with a limited cost increase. The cost of this hardware is comparable to that of simpler solutions based on micro-controllers or digital signal processors, and it is much cheaper than laboratory instrumentation (whose cost is at least a few thousands of dollars).

A schematic diagram of the proposed system for signal acquisition, generation and processing is illustrated in Fig. 6. The voltage and current signals are firstly conditioned to match the specifications of the ADCs, and then are acquired by the

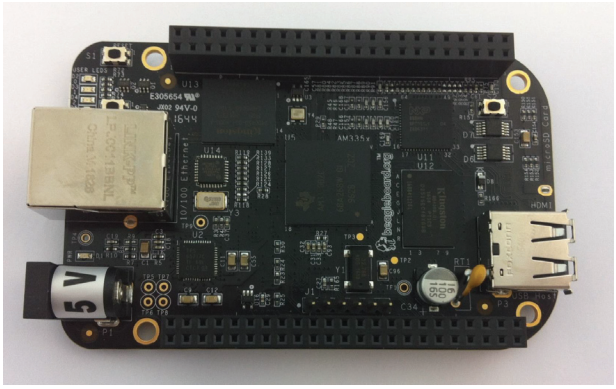

Fig. 5. Photograph of the BeagleBone Black board, which is chosen as the hardware platform for the implementation of signal acquisition, generation and processing, according to the aim of the paper.

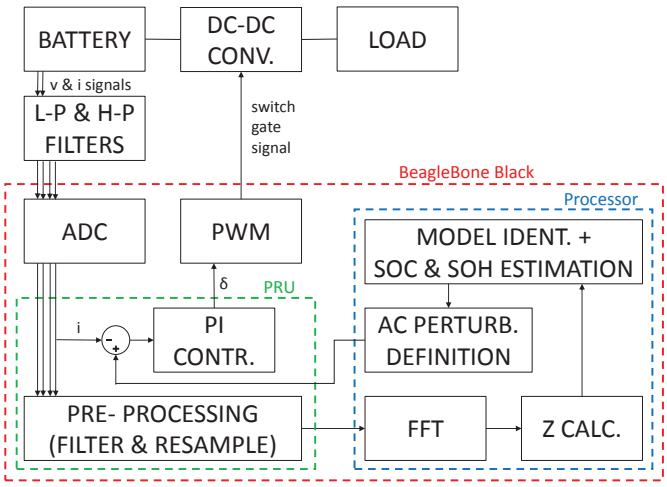

Fig. 6. Schematic diagram of the PWM signal generation and voltage and current signal acquisition and processing, based on the BeagleBone Black board.

BBB. The digital current value is then compared to a predefined reference signal, and a PI controller calculates the required duty cycle for the power converter to follow such reference. The controller can be implemented in the BBB PRU, which also manages the analog inputs and PWM output of the board in hard real-time. Depending on the frequency of the AC perturbation, the PRU may also implement a moving average filter and may down-sample the signals in order to limit the data sent to the processor. The data will be temporarily stored in a memory buffer, waiting to be read by the processor, whose operation is not hard real-time but is fast enough to allow reading the buffer before it is overwritten, on a time scale of tens of milliseconds.

In order to calculate the impedance at the frequency components present in the perturbation signal, the FFT has to be applied to the voltage and current waveforms. However, during the measurement time the battery is discharged and this creates a linear drift in the DC voltage value, superimposed to the AC perturbation, as illustrated in Fig. 7. Considering that

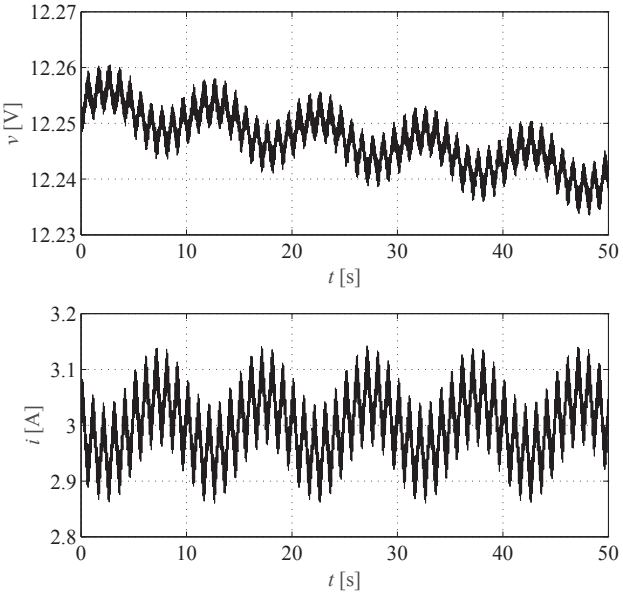

Fig. 7. Battery voltage (upper plot) and current (bottom plot) waveforms with perturbations at 100 mHz, 1 Hz and 10 Hz, showing the linear drift of the DC voltage while the battery is discharged.

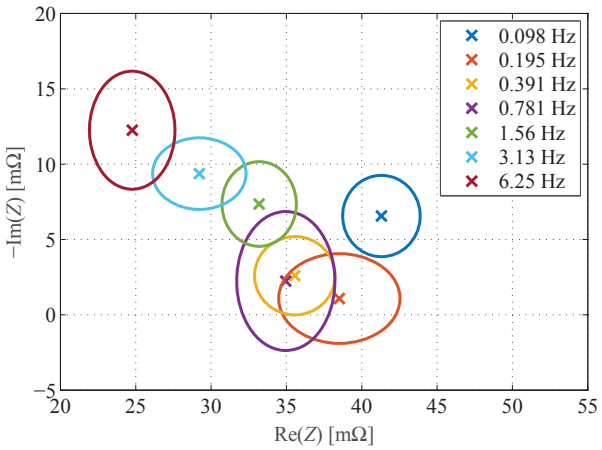

Fig. 8. Battery impedance measured at 7 frequencies in the range from 98 mHz to 6.25 Hz, by using a multi-sine current perturbation. The uncertainty of each impedance value (real and imaginary parts) is calculated in real-time as standard deviation of 10 samples and is plotted as an ellipse around the average value.

the amplitude of the AC voltage perturbation is usually very small, such a drift can give rise to significant errors in the signal frequency spectrum if not compensated. In the example of Fig. 7, the current contains three sinusoidal components, at 100 mHz, 1 Hz and 10 Hz, each of them with an amplitude of 0.05 A which corresponds to a voltage oscillation amplitude of approximately 3 mV; the linear drift in the voltage DC value is -0.25 mV/s and is enough to create errors of approximately 2% and 30% in the impedance calculations at 1 Hz and 100 mHz, respectively. Therefore a linear least-squares fitting in the time domain is implemented in order to remove the linear trend in the voltage waveform before applying the FFT.

IV. Experimental Results

Fig. 8 shows part of the battery impedance spectrum, measured by using a multi-sine current perturbation containing 7 frequency components from 98 mHz to 6.25 Hz, uniformly spaced on a logarithmic scale and each of them with an amplitude of 0.1 A, superimposed to a DC current of 3.0 A. The impedance values are calculated on a time window of 40.96 s and then averaged over 10 windows. In addition to calculating the average, also the standard deviation of the 10 samples is calculated in real-time, in order to have a type-A uncertainty estimate, which in this case is the dominant contribution due to the large noise and random fluctuations affecting these measurements. The standard deviation is calculated on the real and imaginary parts of the impedance separately, and the results correspond to the semi-axes of the ellipses plotted in Fig. 8. Such uncertainty evaluation could be used, e.g., as a weighting factor when fitting the measured data with an equivalent circuit model such as the one reported in Fig. 2, but also to monitor the changes of impedance values during time.

An example of a transient showing a change in the battery impedance is reported in Fig. 9, obtained again at a DC current level of 3.0 A; for sake of simplicity, only one impedance value is reported, measured at 1.56 Hz. The upper plot shows the significant voltage decrease during such a long transient, corresponding to an overall charge variation ΔQ of more than 2.5 Ah (the nominal battery capacity is 7.0 Ah), calculated by integrating the current. The voltage decrease is almost linear during the first half of the transient, but then it becomes nonlinear. This slope change corresponds to a noticeable change in the real part of the impedance in the second half of the transient (as visible in the bottom plot), which creates an increasingly higher voltage drop. Such a variation can be interpreted as an increase in the ohmic resistance, which is indeed expected to change with the SOC in lead-acid batteries [6]. The impedance values reported in Fig. 9 are calculated on time windows of 5.12 s and averaged over 12 windows with a moving average filter. Similarly, the standard deviation σ of the 12 samples is calculated to estimate the impedance uncertainty as described above. The uncertainty band plotted in Fig. 9 corresponds to an interval of $\pm 2\sigma$, which can be used to determine whether any observed change in the impedance is significant or not, with a 95.45% confidence level (assuming Gaussian probability distributions). Based on this, it is possible to confirm that there is an actual change in the real part of the impedance, whereas no significant variations are detected in the imaginary part, in agreement with a variation of the ohmic resistance alone.

V. Conclusions

This paper described a low-cost hardware platform suitable to perform in-situ electrochemical impedance spectroscopy

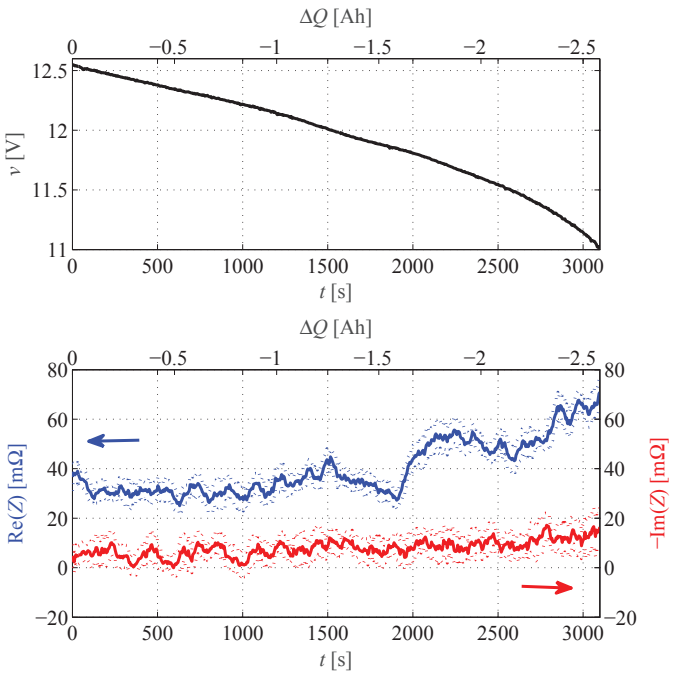

Fig. 9. Battery DC voltage (upper plot), and real (blue) and imaginary (red) parts of the impedance at 1.56 Hz (bottom plot), measured during a discharge transient at 3.0 A constant current. The uncertainty bands in the bottom plot (dotted lines) correspond to a $\pm 2\sigma$ type-A uncertainty, calculated as moving standard deviation over 12 impedance values.

on batteries employed in commercial applications, by using the already available DC-DC converter to introduce AC perturbations superimposed to the DC current and voltage, at the desired frequencies in a wide range from millihertz to kilohertz. A BeagleBone Black board was shown to be an appropriate hardware solution to control the converter, acquire and process the current and voltage measurements in the time and frequency domains, and calculate the impedance values and their uncertainty in real-time, because it combines hard real-time programmable units with a powerful processor, it supports operating systems with a user-friendly graphical interface, and its cost and size are likely to be affordable in a commercial application.

The design of the hardware (including the power converter) used to test the proposed approach was firstly presented. Experimental results were also reported to demonstrate that the measurement system is accurate enough to detect impedance variations during time, e.g. associated with a change in the battery SOC and/or SOH.

REFERENCES

[1] X. Luo, J. Wang, M. Dooner and J. Clarke, "Overview of current development in electrical energy storage technologies and the application potential in power system operation", *Applied Energy*, vol. 137, pp. 511-536, 2015.

[2] A. Jossen, "Fundamentals of battery dynamics", *Journal of Power Sources*, vol. 154, pp. 530-538, 2006.

[3] W. Waag, S. Käbitz and D. U. Sauer, "Experimental investigation of the lithium-ion battery impedance characteristic at various conditions and aging states and its influence on the application", *Applied Energy*, vol. 102, pp. 885-897, 2013.

[4] D. Andre, M. Meiler, K. Steiner, Ch. Wimmer, T. Soczka-Guth and D. U. Sauer, "Characterization of high-power lithium-ion batteries by electrochemical impedance spectroscopy. I. Experimental investigation", *Journal of Power Sources*, vol. 196, pp. 5334-5341, 2011.

[5] U. Tröltzsch, O. Kanoun and H.-R. Tränkler, "Characterizing aging effects of lithium ion batteries by impedance spectroscopy", *Electrochimica Acta*, vol. 51, pp. 1664-1672, 2006.

[6] F. Huet, "A review of impedance measurements for determination of the state-of-charge or state-of-health of secondary batteries", *Journal of Power Sources*, vol. 70, pp. 59-69, 1998.

[7] M. Shirazi, J. Morroni, A. Dolgov, R. Zane and D. Maksimovic, "Integration of frequency response measurement capabilities in digital controllers for DC-DC converters", *IEEE Trans. on Power Electronics*, vol. 23, no. 5, pp. 2524-2535, 2008.

[8] D. Depernet, O. Ba and A. Berthon, "Online impedance spectroscopy of lead acid batteries for storage management of a standalone power plant", *Journal of Power Sources*, vol. 219, pp. 65-74, 2012.

[9] W. Huang and J. A. Abu Qahouq, "An online battery impedance measurement method using DC-DC power converter control", *IEEE Trans. on Industrial Electronics*, vol. 61, no. 11, pp. 5987-5995, 2014.

[10] A. Densmore and M. Hanif, "Determining battery SoC using electrochemical impedance spectroscopy and the extreme learning machine", *IEEE 2nd Int. Future Energy Electronics Conference*, Taipei, Taiwan, 1-4 Nov. 2015, pp. 1-7.

[11] M. A. Varnosfaderani and D. Strickland, "Online impedance spectroscopy estimation of a battery", *18th European Conference on Power Electronics and Applications*, Karlsruhe, Germany, 5-9 Sep. 2016, pp. 1-10.

[12] E. Din, C. Schaef, K. Moffat and J. T. Stauth, "A scalable active battery management system with embedded real-time electrochemical impedance spectroscopy", *IEEE Trans. on Power Electronics*, vol. 32, no. 7, pp. 5688-5698, 2017.

[13] G. Dotelli, R. Ferrero, P. Gallo Stampino, S. Latorrata and S. Toscani, "PEM fuel cell drying and flooding diagnosis with signals injected by a power converter", *IEEE Trans. on Instrumentation and Measurement*, vol. 64, no. 8, pp. 2064-2071, 2015.

[14] G. Dotelli, R. Ferrero, P. Gallo Stampino, S. Latorrata and S. Toscani, "Low-cost PEM fuel cell diagnosis based on power converter ripple with hysteresis control", *IEEE Trans. on Instrumentation and Measurement*, vol. 64, no. 11, pp. 2900-2907, 2015.

[15] N. Katayama and S. Kogoshi, "Real-time electrochemical impedance diagnosis for fuel cells using a DC-DC converter", *IEEE Trans. on Energy Conversion*, vol. 30, no. 2, pp. 707-713, 2015.

[16] G. Dotelli, R. Ferrero, P. Gallo Stampino and S. Latorrata, "Analysis and compensation of PEM fuel cell instabilities in low-frequency EIS measurements", *IEEE Trans. on Instrumentation and Measurement*, vol. 63, no. 7, pp. 1693-1700, 2014.